Bidirectional River-Floodplain Connectivity During Combined Pluvial-Fluvial Events

Nelson Tull[1], Paola Passalacqua[1], Hima J. Hassenruck-Gudipati[2], Shazzadur Rahman[1*], Kyle Wright[1], Jayaram Hariharan[1], and David Mohrig[2]

[1]Department of Civil, Architectural, and Environmental Engineering, Center for Water and the Environment, University of Texas at Austin, Austin, TX, USA
[2]Department of Geosciences, Jackson School of Geosciences, University of Texas at Austin, Austin, TX, USA

Key Points:

- Field data and modeling show distinct signals of pluvial and fluvial flooding
- Floodplain residence times change dramatically between pluvial and fluvial phases of the storm
- Numerical model resolution has a local effect on floodplain channel conveyance, but has little influence on overall residence times

*Walter P. Moore, Dallas, TX

Corresponding author: Paola Passalacqua, paola@austin.utexas.edu

Abstract

Hydrological connectivity controls the lateral exchange of water, solids, and solutes between rivers and floodplains, and is critical to ecosystem function, water treatment, flood storage and attenuation, and geomorphic processes. Hydrological connectivity has been studied extensively, typically through the lens of river-driven flooding, but in regions prone to heavy rainfall, the timing and magnitude of lateral exchange may be altered dramatically by local flooding on the floodplain. We collected field measurements of flow depth and velocity in the Trinity River floodplain in coastal Texas (USA) during Tropical Storm Imelda (2019), which produced up to 75 cm of rainfall locally. We developed a two-dimensional, depth-averaged hydrodynamic model at high resolution for a section of the Trinity River to replicate floodplain hydrodynamics and determine the impact of floodplain channels on connectivity. We employed Lagrangian particle routing to quantify how residence times and particle velocities changed as flooding shifted from rainfall-driven to river-driven. Our results show that heavy rainfall initiated lateral exchange before river discharge reached flood levels. The presence of rainwater also reduced floodplain storage, causing river particles to be confined to a narrow corridor on the floodplain, while rainwater residence times were increased from the backwater effect of river flow through the floodplain. Finally, while the resolution of floodplain channels is important locally, it does not affect as much the overall floodplain behavior. This study provides evidence of the added complexity of floodplain hydrodynamics under conditions of heavy rainfall, with implications for sediment deposition and nutrient removal during floods.

Plain Language Summary

Unaltered river floodplains can support diverse ecosystems, reduce flooding, and remove nutrients from river water. Floodplains near the coast are particularly important, as they typically experience more frequent flooding. Floodplain function relies on a high degree of connectivity with the river, where water can move easily through the floodplain during high river stages. Our study explores the ways in which heavy rainfall on a floodplain impacts this connectivity. We collected flow measurements in the Trinity River floodplain (Texas, USA) during Tropical Storm Imelda in 2019 that show how flow can change direction as a flood transitions from rainfall-driven to river-driven. We coupled a hydrodynamic model with a particle tracking module to see how particles in the water might move through the floodplain during this transition. We found that the average time a particle spent in the floodplain changed significantly after the rain in the model stopped. We also noticed that rainwater tended to remain in the floodplain for much longer than river water, especially after the rain stopped. This study describes the various interactions that can occur between local rainfall and river flooding, and moves toward a better understanding of sediment and nutrient transport through floodplains.

1 Introduction

River floodplains play a fundamental role in flood storage, nutrient cycling, sediment retention, and in general provide support for diverse ecosystems (Ward et al., 1999; Melack & Forsberg, 2001; Kondolf et al., 2006; Roley et al., 2012; Noe et al., 2013; Kufel & Leśniczuk, 2014). Floodplains are complex and heterogeneous, and their structure and function are highly dependent on their degree of connectivity with the river (Hughes et al., 2001; Harvey & Gooseff, 2015; Gurnell et al., 2016; Covino, 2017). Topographic and hydrologic controls on connectivity have been described for the largest river-floodplain systems using satellite imagery (Lesack & Melack, 1995; Mertes et al., 1995; Mertes, 1997; Alsdorf et al., 2007; Trigg et al., 2012; Lewin & Ashworth, 2014; Park & Latrubesse, 2017), and more recently for medium-size rivers using lidar data and numerical modeling (David et al., 2017; Czuba et al., 2019; Byrne et al., 2019). However, river-floodplain connectivity is poorly understood when hydrodynamics are partially driven by local rainfall. Mixing of rainfall and river floodwaters

has been observed and discussed for very large river floodplains (Mertes, 1997; Alsdorf et al., 2007; Day et al., 2008; Rowland et al., 2009; Trigg et al., 2012), where floodplain channels are at a large enough scale to be sensed remotely, and the flood wave occurs over much longer time scales (Junk et al., 1989). But for medium-size rivers, flood waves are less predictable, and floodplain features are often too small to detect using satellite imagery. The goals of this study are to show (a) the impact of local rainfall on floodplain residence times, flow directions, and connectivity within the floodplain, and (b) to determine the role of floodplain channel scale in facilitating river-floodplain exchange.

Floodplain topography has been shown as a key control on mixing of local runoff and river waters in large floodplain systems, where most mixing tends to occur outside of channel features (Lesack & Melack, 1995; Mertes et al., 1995; Mertes, 1997; Trigg et al., 2012). Flow within these floodplain channels can be bidirectional due to the advancing and receding of the flood wave and the timing of rainfall runoff on the floodplain (Alsdorf et al., 2007; Day et al., 2008; Rowland et al., 2009). For smaller river systems as well, sub-bankfull discharges can result in floodplain inundation that is limited spatially by the extent of lateral floodplain channels in the system (Kupfer et al., 2015; Czuba et al., 2019). Pluvial flooding may enhance connectivity within the floodplain by bringing inundation, and potentially nutrients and sediment, to areas of the floodplain that would otherwise be out of reach for river waters. On the other hand, if intense enough, pluvial flooding can develop a water surface gradient moving from floodplain to channel, which may reduce flux into the floodplain (Day et al., 2008). It is common that fluvial and pluvial flooding at a site are not coincident in time, as a result of a storm moving slowly over a watershed, and thus the interaction between the two flooding modes may be complex in space and time. Recent studies of river-floodplain connectivity have used unsteady numerical models to show how floodplain hydrodynamics evolve with the rising and falling of a river flood wave (Byrne et al., 2019; Chen et al., 2020), but no study has used numerical modeling to analyze the interaction of fluvial and pluvial flooding. Furthermore, no study to-date has presented field measurements of floodplain flow that show this interaction.

The interaction of pluvial and fluvial flooding may have significant impacts on residence time, flow direction, and the overall extent of hydrological connectivity in river-floodplain systems, all of which can be drivers of dissolved nutrient sequestration (Mann & Wetzel, 1995; Tockner et al., 1999; Aufdenkampe et al., 2011; Noe & Hupp, 2005; Noe et al., 2013; Wolf et al., 2013; Cheng & Basu, 2017) and sediment deposition (Tockner et al., 1999; Verhoeven et al., 2001; Schulz et al., 2003; Day et al., 2008; Trigg et al., 2012; Juez et al., 2019) in floodplains. Sediment deposition depends on local availability from the river, as well as flow velocity distributions across the floodplain to advect the sediment (Marriott, 1992; Asselman & Middelkoop, 1995), while dissolved nutrients require sufficient contact time to be removed from floodwaters via biogeochemical processes (Tockner et al., 1999; Noe et al., 2013; Cheng & Basu, 2017). The depositional environments of lowland river floodplains are understood to provide conditions conducive to these processes, yet it is unknown how conditions change when pluvial flooding is substantial.

In this study we show how pluvial flooding impacts residence time distributions and flow patterns in a low-gradient river-floodplain system by using the lower Trinity River (Texas, USA) as a study site. To our knowledge this is the first modeling study of pluvial flooding in the context of hydrological connectivity. We present flow depth and velocity measurements collected during Tropical Storm Imelda (2019) in the Trinity River floodplain that show flow reversals as floodplain inundation transitioned from rainfall-driven to river-driven. We then develop several two-dimensional, depth-averaged numerical models with varying grid resolution to replicate the observed hydrodynamics during the storm and determine the role of floodplain channel scale on river-floodplain connectivity. Next, we employ a Lagrangian particle routing tool on the unsteady model flow fields to quantify how rainfall and channel processes impact residence time distributions and flow patterns in floodplains.

The outline of the manuscript is as follows. Section 2 describes the characteristics of the lower Trinity River study site, including a description of the elevation data used for this study. Section 3 introduces Tropical Storm Imelda, the test-case event, and the hydrodynamic data collected in the Trinity River floodplain in 2019 during the storm. Section 4 introduces the ANUGA (Eulerian) and *dorado* (Lagrangian) models, and describes the modeling approach. Section 5 presents the results of the study, including the unique impacts of rainfall on floodplain hydrodynamics. Section 6 provides a discussion of implications for floodplain services and for future modeling studies of river-floodplain connectivity. Lastly, Section 7 summarizes the major findings of the study.

2 Study Area: The Trinity River

2.1 Site Description

The Trinity River basin ($40,000$ km^2) extends from its outlet in Trinity Bay into north-central Texas (Figure 1A). The area of investigation spans about 10.5 river kilometers (rkm) of the lower basin in Liberty County, between Liberty and Wallisville, TX. The study area is within the river's backwater reach (BWR), which is recognized by the asymptotic approach of the water surface elevation to the surface elevation of the receiving basin. Under low-discharge conditions, the BWR begins approximately 15 rkm upstream of the study area (Figure 1B) (Mason & Mohrig, 2018). As is typical in such systems, stage change between low and flood flows is smaller in the BWR, with variations in reach-average flow velocity primarily accommodating water discharge changes.

As the river transitions from a normal flow regime to the BWR, the channel morphodynamics responds to the adjustments in flow conditions and the transport of solids. This transition coincides with downstream narrowing and deepening of the channel. Rates of channel-bend migration decrease in the downstream direction, as do the size and shape of point bars, and grain size of bed material (Smith et al., 2020). Similarly, the overbank conditions vary in accordance with the transition to the BWR. For example, upstream of the BWR the floodplain is active and largely remains dry during low and moderate flow conditions, but is inundated during floods, when water emerges from channel confinement and spreads across the floodplain. In contrast, the BWR is characterized by a wetland environment due to its relatively low elevation and is prone to inundation by moderate river discharges. Because of these characteristics, connectivity is greater in the study reach compared to upstream, and floodplain channels are more commonplace and pronounced. This connectivity causes a "leakiness" in the system, which is supported by the large decrease in average annual peak discharge from Liberty ($2,477$ m^3/s) to Wallisville (756 m^3/s) observed between years 2015 and 2020.

Like many fluvial-deltaic systems worldwide, the Trinity is not free of anthropogenic influences. However, the study reach is unaffected by significant modifications such as containment levees, wing dykes, and revetments; thus, the river is able to operate unhindered within its valley. The Livingston Dam (upstream of our study area) is a run-of-river dam that impacts the river geomorphology for the first 50-60 rkm downstream of the structure (Phillips et al., 2004; Phillips & Slattery, 2007; Smith & Mohrig, 2017). Beyond this point, sediment mining from the bed and banks of the river re-establishes the bed-material load (Smith & Mohrig, 2017) and no change in channel geometry and kinematics has been observed since reservoir filling.

The model domain boundary shown in Figure 1C was chosen for three main reasons. First, the domain contains three of the field observation sites (see Section 3.2) that recorded data during Tropical Storm Imelda. Second, and related to the first, the floodplain topography in this area features many channels of various sizes that connect the river to the floodplain. Floodplain channel sizes range from small, 1-2 m channels barely detectable in the lidar, to larger, 8-10 m channels that are lower in elevation and most likely play

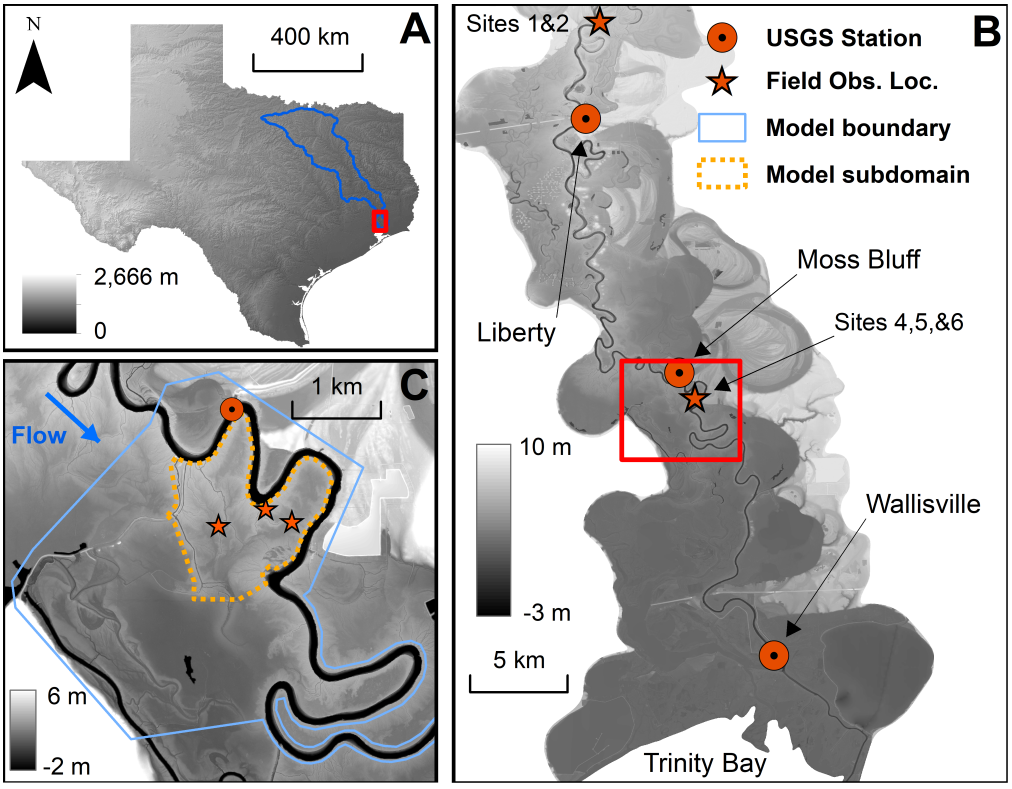

Figure 1. Elevation maps of the Trinity River study area. (A) Location of the Trinity River basin in Texas. (B) Lidar data for Trinity River floodplains between Liberty (upstream) and Wallisville (downstream), including locations of field observation sites. (C) Boundary of model domain used in this study, along with locations of three field observation sites within the study area (Sites 4, 5, and 6, from left to right). The downstream boundary of the model domain extends to Wallisville, but is not shown here.

a larger role in river-floodplain exchange. The complex floodplain topography makes this location interesting to study. Third, the domain boundary needed to be limited in space, as the high-resolution modeling needed to resolve the smallest channels requires significant computational resources.

2.2 Elevation Data

All elevation data and references to elevation in this manuscript are relative to the NAVD88 datum. The elevation data shown in Figure 1 were derived from lidar measurements collected in February and March of 2017 as part of the Texas Strategic Mapping Program. Data were acquired and processed by the Sanborn Map Company with third party quality assurance and control provided by AECOM. Collection took place during the leaf-off season in Texas. The reported horizontal and vertical accuracy of the lidar are 0.25 and 0.29 m, respectively.

The lidar data were interpolated to a bare-earth digital elevation model (DEM) at 1-m resolution. Small voids in the floodplain lidar were interpolated using a second-degree polygon plane fit through the existing data. Larger voids corresponding to floodplain ponds, major channels, and oxbows were interpolated similarly but subtracted by 5 m as a bathymetry approximation. River bathymetry measurements were taken by the Trinity River Authority

in 2017, along four longitudinal profiles at transects spaced every 400 m on average (the river width varies between 80 and 100 m). The bathymetry was interpolated to a 10-m grid, and patched together with the lidar DEM using the Raster to Mosaic tool in ArcGIS. Finally, the boundary between the datasets was linearly interpolated between the edge of the lidar data and the closest longitudinal bathymetry profile.

3 Tropical Storm Imelda

3.1 Storm Background

Tropical Storm Imelda (2019) was a major rainfall event that produced over 75 cm of precipitation across several counties in the area surrounding Houston, TX (Latto & Berg, 2020). Imelda made landfall near Freeport, TX on 17 September 2019 as a tropical storm, before quickly weakening to a tropical depression as it moved slowly northward through Houston, TX and subsequently across the lower Trinity River watershed. The storm further degenerated to a trough by 19 September, at approximately 160 km north-northeast of Houston, where it continued to dissipate and move northward. The highest recorded rainfall total from Imelda was 112 cm, which made it the fifth wettest tropical cyclone ever recorded in the contiguous United States.

Eastern Texas experienced widespread pluvial flooding during this period. While the lower Trinity River watershed received much of this rainfall, including up to 75 cm at the study site, the river stage at the USGS gaging station at Liberty peaked just below the official flood stage as defined by the National Weather Service. A sub-bankfull flood event is suitable for analyzing river-floodplain connectivity, as floodplain channels are activated and responsible for any lateral exchange that occurs, and floodplain inundation is heterogeneous. The timing mismatch of the pluvial and fluvial flooding peaks, along with the sheer volume of precipitation, created an opportunity for competition between river and floodplain water worth investigating.

3.2 Field Data Collection

During August 2019, six outdoor trail cameras, six measuring rods, six water level loggers, and four tilt current meters were installed at various floodplain locations along the Trinity River (Figure 1). The loggers recorded water level every six minutes, while the tilt current meters recorded flow speed and direction every minute. The cameras took a photograph of the installation plus measuring rod every five minutes, night and day. The instruments were left in the field until February 2020, and successfully collected data during Tropical Storm Imelda. Sites 1, 2, and 3 were located north of Liberty near the bend indicated in Figure 1B. Site 1, located in a large floodplain channel, collected water level velocity readings, while Site 2, located in a shallow levee-traversing channel, collected water levels only. Instruments at Site 3 were destroyed during the storm. Sites 4, 5, and 6 were all located in the study area shown in Figure 1C. Sites 4 and 6 collected both water level and velocity readings, while Site 5 collected water levels only. Site 4 instruments were located in a floodplain channel roughly 930 m from the Trinity River (measured along the channel). Site 5 was located on a different floodplain channel, just 50 m from the river. Site 6 was located at the terminus of the same channel monitored by Site 5. At Site 6 a small internal delta was building out from the mouth of the floodplain channel into the adjacent, small floodplain basin with perennial standing water. Sites 5 and 6 were located on a channel connected to the river bend immediately upstream from the USGS gaging station at Moss Bluff (Figure 1). The field instrument locations provided a diverse set of topographic and hydrologic conditions for observing the patterns of rainfall and river flooding that occurred during Imelda.

4 Modeling Approach

This study employed a numerical model and a Lagrangian particle routing tool to analyze the hydrodynamics of the Trinity River floodplain during Tropical Storm Imelda. First, a numerical model of near-constant grid resolution was developed for the study reach. Then a set of additional unstructured meshes was developed for the same domain, where each mesh has increased resolution only within the floodplain region of interest; that is, the floodplain and channel banks surrounding the three field instruments (Figure 1C). Simulations were run on each mesh and results were compared to field measurements of depth in the floodplain. Flow fields from the model simulations were used to model passive particle transport and compute average particle speeds and residence times across the floodplain. Through these methods, we infer the relative impact of pluvial and fluvial flooding, as well as the role of floodplain channel scales, on floodplain hydrodynamics.

4.1 ANUGA Model Development

The ANUGA hydrodynamic model was used for numerical modeling in this study. ANUGA is an open-source program developed by researchers at the Australian National University and Geoscience Australia (Roberts et al., 2015). It solves the shallow-water equations using unstructured meshes and a finite-volume numerical scheme. Details of the numerical scheme can be found in Nielsen et al. (2005), Mungkasi and Roberts (2011), and Mungkasi and Roberts (2013). ANUGA was the model of choice for several reasons, including: (*i*) it is open-source and therefore easy to control and customize; (*ii*) the finite-volume method conserves mass and momentum along the wetting-drying front; (*iii*) it uses unstructured meshes; (*iv*) it scales efficiently in high-performance computing environments; and (*v*) it employs a variable time step. The flexibility of the unstructured mesh allows for higher model resolution in areas of higher priority, while offering reduced resolution in areas of less concern. This, along with the parallel capabilities and variable time step, reduces the computational resources needed for model simulations, which is important for an application where near-lidar-scale grid resolution was used.

The model domain boundary (shown in Figure 1C) was delineated to incorporate all channel and overbank areas contributing flow to the floodplain area of interest, while using the smallest domain possible for computational reasons. The "control" domain for this study consisted of an unstructured mesh with a constant average element edge length of 20 m, and 78,752 total elements. The 20 m element size is approximately one-fifth of the width of the main channel, which provided a sufficient representation of the channel cross-section geometry. 20-m resolution was too coarse to resolve most floodplain channels along the Trinity, and was only able to resolve longer-range elevation changes, such as a floodplain basin or a group of nearby floodplain channels that are averaged collectively into a smooth low area.

Following development of the 20-m mesh, in which all mesh elements were of a constant size at 20 m per side, three additional meshes were developed. Each mesh had the same outer boundary, and the same resolution across the majority of the domain. The difference lies in the subdomain area delineated in Figure 1C, where the bends and floodplain channel networks contributing to the three field data sites were represented with higher mesh resolution. The three meshes had mean resolutions within the subdomain of 10 m, 5 m, and 2 m, with total element counts of 129,051; 269,361; and 1,308,101; respectively. For each mesh, elements were uniform in size within the floodplain subdomain, but a buffer region was present where the mesh elements transitioned in size between the subdomain and the base, 20-m resolution. 10 m was chosen as the upper resolution bound because it was approximately the scale of the largest floodplain channels observed in the lidar. Ideally, the highest resolution mesh would reach the scale of the 1-m DEM, and provide the best representation of floodplain channel geometry. However, 2 m was found to be the computational limit. The time step required by such small elements, especially those located along

cut-banks near the main channel thalweg, was very small. Further increasing the resolution to 1 m in these areas would result in numerical instability or prohibitive computation time. Although there are visible features in the lidar less than 2 m in width, the majority of these channels are located on top of levees, where only overbank flow would activate them.

The upstream and river-left boundaries were modeled as no-flow (reflective) boundaries. The downstream domain boundary extended approximately 13.4 rkm from the study site to Wallisville, TX. This extension included only the river channel itself, and was appended to the domain to provide a sufficient distance between the study site and the downstream river boundary condition. A constant water surface elevation (WSE) of 0.7 m (NAVD88) was imposed at the downstream boundary, representing the mean WSE measured at the Wallisville USGS gaging station in the days preceding the storm. The longitudinal boundaries along the channel levees of this extension were transmissive boundaries to allow for any overbank flow to pass out of the domain. The boundary passing through the river-right floodplain at the downstream end was modeled as a quasi-transmissive boundary. This was a time-varying, zero-momentum boundary with a WSE always equal to 5 cm below the current WSE in the domain adjacent to the boundary. Several boundary conditions were applied at this location, including a completely transmissive boundary and a constant WSE boundary, but these conditions overestimated and underestimated drainage from the floodplain, respectively. The quasi-transmissive boundary was used as an approximation to the water surface slope moving through the floodplain.

The DEM described in Section 2.2 was applied to mesh vertices via a least-squares fit with minimal smoothing. Elevations at mesh element centroids were computed as the average of the three vertices, creating a discontinuous, piecewise-constant elevation surface used by the ANUGA "DE1" flow algorithm (Davies & Roberts, 2015). Friction forcing was applied to the domain as two constant Manning's n values: 0.025 within the main channel, and 0.075 in the floodplain. These values were chosen based on guidance from literature (Chow, 1959), intuition from field visits and site photographs, and model calibration. River floodplains are clearly heterogeneous, with dense forested areas expected to have a higher flow resistance than the channelized portions that are the focus of this study. However, analyzing frictional heterogeneity in the floodplain (and channel) is beyond the scope of this study. Future work may involve a more complex distribution of friction based on analysis of aerial images, specifically vegetation color and density, and topographic images, where surface curvature may be correlated to flow resistance.

The model was run over a 10-day period, beginning at 0000 Central Time on 17 September 2019 and lasting through 26 September. The model was forced using discharge and rainfall data collected at the Liberty USGS gage during Tropical Storm Imelda. The base flow recorded at Liberty at the starting time was 52 m^3/s, while the peak discharge from Imelda was 793 m^3/s, occurring at 1100 on 21 September. The Liberty gage hydrograph was calibrated to match the observed WSE in the channel, as the rating curve changes significantly in the BWR and applying a dynamic downstream boundary condition carries too much uncertainty. The hydrograph used to force the model is shown in Figure 2, with an initial discharge of 32 m^3/s and a peak discharge of 681 m^3/s. Rainfall measurements at Liberty consisted of three distinct passovers of tropical storm bands, corresponding to the spikes in water levels on the floodplain seen in Figure 2. The data show the first rainfall band arriving at 2100 CT on 18 September and the third band ending at 1530 on 19 September. The combined depth of rainfall added to the model from the three bands was 75.3 cm. This depth corresponds to a total volume of 1.0×10^6 m^3 added to the domain over an 18.5-hour period. A less intense, background rainfall rate was also added to the model to replicate the steady accumulation of water observed in the field data prior to the tropical storm bands.

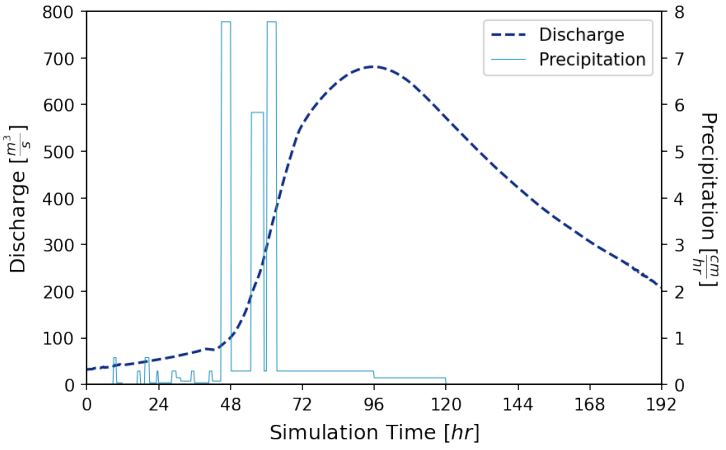

Figure 2. Hydrograph and hyetograph for Tropical Storm Imelda as applied to the numerical model. The period of intense rainfall occurring from storm bands preceded peak river flooding by about 30 hours.

4.2 Quantifying Residence Times with *dorado*

dorado (Hariharan et al., 2020) is an open-source, Lagrangian particle routing package that uses a D-8 walk algorithm (Pearson, 1905) to simulate passive particle transport through hydrodynamic flow fields on regular grids. Here we provide a brief description of *dorado*; for more information see Hariharan et al. (2020) and the *dorado* documentation. The particle walk algorithm is weighted by local flow direction and water depth, in a manner similar to that of the DeltaRCM model (Liang, Voller, & Paola, 2015; Liang, Geleynse, et al., 2015). For a given grid cell, the downstream direction F^* is computed by a weighted combination of water surface slope (F_{sfc}) and discharge (F_{int}) unit vectors:

$$F^* = \gamma F_{sfc} + (1-\gamma) F_{int} \tag{1}$$

where the parameter γ is specified by the user depending on the nature of transport. Particles are then routed based on orientation to the mean flow direction and the depth in each cell:

$$w_i = \frac{h_i^\theta \ \max(0, F^* \cdot d_i)}{\Delta_i} \tag{2}$$

where F^* is the local flow direction computed in Equation 1, d_i is the unit vector pointing to downstream cell i, Δ_i is the Euclidian distance to downstream cell i, h_i is the depth of downstream cell i, and the exponent θ is a weighting parameter specified by the user (Liang, Voller, & Paola, 2015; Hariharan et al., 2020). The default value of θ is 1.0, which routes particles proportionally based on flow depth under the assumption that deeper cells receive more flow than their shallower neighbors (in the absence of vertical model resolution). The particle routing in this study uses $\gamma = 0.05$ and $\theta = 1.0$, where routing weights depend mostly on discharge, and therefore the analysis and discussion that follows can be thought of conceptually as water solute transport.

dorado tracks individual paths and travel times of particles as they are routed through a flow field. An effective particle travel distance is computed for each iteration, defined by the Euclidian distance traveled to one of the surrounding eight grid cells projected onto the

mean flow vector. The particle travel time $T_{p,i}$ between two cells is then back-calculated from the effective travel distance and local flow velocities, with a dispersion coefficient applied that allows $T_{p,i}$ to vary stochastically up to 10 percent from the mean velocity.

In a steady flow field, a sufficient number of particles initialized at the domain inflow location and routed through the domain can provide a probabilistic, spatial distribution of particle paths. All hydraulically-connected locations in the flow field have some probability of having a particle pass through. The total travel time for each particle can be computed, and the average travel time for all particles passing through a stationary part of the domain can be computed as well. Particle travel paths are limited, however, to the instantaneous WSE gradient and discharge in the steady flow field, which may be only representing a particular snapshot in time. The flow field may show certain areas of the floodplain as connected hydraulically, but the instantaneous directionality of the water surface may prevent particles from reaching those areas.

A flow field that changes through time, due to the rising and falling of the flood wave or unsteady precipitation on the floodplain, creates an environment where potential particle paths are highly dependent on when and where particles enter the floodplain from the river. For example, a particle will not move from river to floodplain until the river stage reaches an elevation higher than the elevation of the deepest floodplain channels. Even then, if the floodplain is already inundated from rainfall the gradient may not allow river flow into the floodplain. Only at a higher river stage might the flow direction change. Routing particles through an unsteady flow field is critical to understanding these river-floodplain interactions.

The ANUGA model depth, stage, and momentum outputs were interpolated to a 2-m raster grid, and a new particle "cohort" consisting of 1,000 particles was initialized in the domain every 15 minutes of model simulation time. Two classes of particles were analyzed: river particles and floodplain particles. All river particle cohorts were initialized at the inlet of the domain, while floodplain particles were seeded randomly throughout the floodplain in grid cells with depth greater than 20 cm. Separating particles into these two classes is necessary for distinguishing between patterns of rainfall and river flood processes. Floodplain particles were initialized beginning at simulation hour 45 (the onset of intense rainfall, see Figure 2), while river particles were initialized at simulation hour 60, as flow does not move from river to floodplain until sometime after hour 60. All particle cohorts were routed through the model flow field until simulation hour 120. With 1,000 particles per 15 minutes, the total number of river particles tracked was 240,000, and the total number of floodplain particles was 300,000.

Particle dynamics were quantified in two ways: velocity distributions and residence time distributions. Velocity distributions show the spatial extent of particle paths, as well as the average speed at which particles move through each 2-m grid cell in the model domain. The average time a particle spends in cell (x, y) is calculated as follows:

$$t_{avg,xy} = \sum_{p=1}^{N_p} \frac{0.5 \times (T_{p,i,xy} + T_{p,i+1,xy})}{N_{p,i,xy}} \tag{3}$$

where N_p is the total number of particles, the numerator is the average of travel times for particle p as it entered (i) and as it left ($i+1$) cell (x, y), and $N_{p,i,xy}$ is the number of times a particle entered cell (x, y). The array is masked for $N_{p,i,xy} = 0$. Then the average flow speed $V_{avg,xy}$ is:

$$V_{avg,xy} = \frac{dx}{t_{avg,xy}} \tag{4}$$

where dx is the cell size. A Gaussian smoothing filter with standard deviation of 0.7 was applied to the $V_{avg,xy}$ array to account for cases of strongly unequal particle visits between nearby cells due to the stochasticity involved in modeling a finite number of particles.

Particle residence time distributions are calculated in the form of the cumulative exit age distribution $F(t)$ (Benjamin & Lawler, 2013):

$$F(t) = \int_0^t \frac{dN_p/dt}{N_{p,tot}} dt \tag{5}$$

where $N_{p,tot}$ is the total number of particles that enter a control volume, dN_p/dt is the rate at which particles exit, and at $t = \infty$, $F(t) = 1$. For this study, we define the control volume as the entire river-right floodplain in the model domain. Rather than observe the rate at which particles leave the floodplain, since we do not necessarily know when particles entered the floodplain, we instead track individual particle travel times beginning when they enter (or are seeded in) the floodplain, and ending when they leave:

$$t_p = \sum_{i=1}^{N_i} T_{p,i} \tag{6}$$

where t_p is the total travel time for particle p within the floodplain boundary, N_i is the number of iterations performed while within the boundary, and $T_{p,i}$ is the travel time for each iteration. All values of t_p are sorted in ascending order, and then $F(t_p)$ is simply the cumulative fraction of particles that spent less than t_p in the domain.

5 Results

5.1 Field Observations of Water Level and Velocity

Data collected during Tropical Storm Imelda showed a clear separation of floodplain inundation due to rain and inundation due to rising river stage (Site 5, Figure 3A). Since the precipitation was centered over the site, the floodplain response to precipitation always preceded that tied to river stage. Still, flooding patterns varied depending on specifics of the monitored location. At Site 5, the first day of the storm saw water levels rise and fall with each sequential rain band before the river WSE had risen to the elevation of the floodplain channel (Figure 3A). At the start of the second day, the river stage had risen to the point that river water contributed to flow in the floodplain channel. For the following three days peak flow depth tracked river stage until stage fell below water levels on the floodplain.

The other field sites showed diverse flow patterns. At Site 1, water in the floodplain channel flowed out to the river throughout the entire event, with peak velocity tied to peak rainfall, not river stage (Figure 3B and C). Data collected at Site 2 on a high levee showed that water always flowed down the levee and away from the river, but this flow was driven entirely by rainfall, as river stage was insufficient to overtop the levee. At Site 6 in the study area, water flowed out to the river through the nearby floodplain channel during peak rainfall and then reversed course, flowing back onto the floodplain with peak velocity tied to peak river stage (Figure 3B and C). Velocities were lower at Site 6 because it was situated at the transition between the mouth of a floodplain channel and its connected, small floodplain basin, and flow directions were also sensitive to rainwater draining to the site from several directions. Less than 1 km away in the Site 4 floodplain channel farther from the river, water always flowed away from the river into the floodplain interior (Figure 3B and C).

Imagery collected by the time-lapse cameras confirmed these observations, showing a rapid rise in water level soon after the beginning of rainfall, followed by a pattern of drainage consistent with saturated soil conditions throughout the event. Saturated soils are common

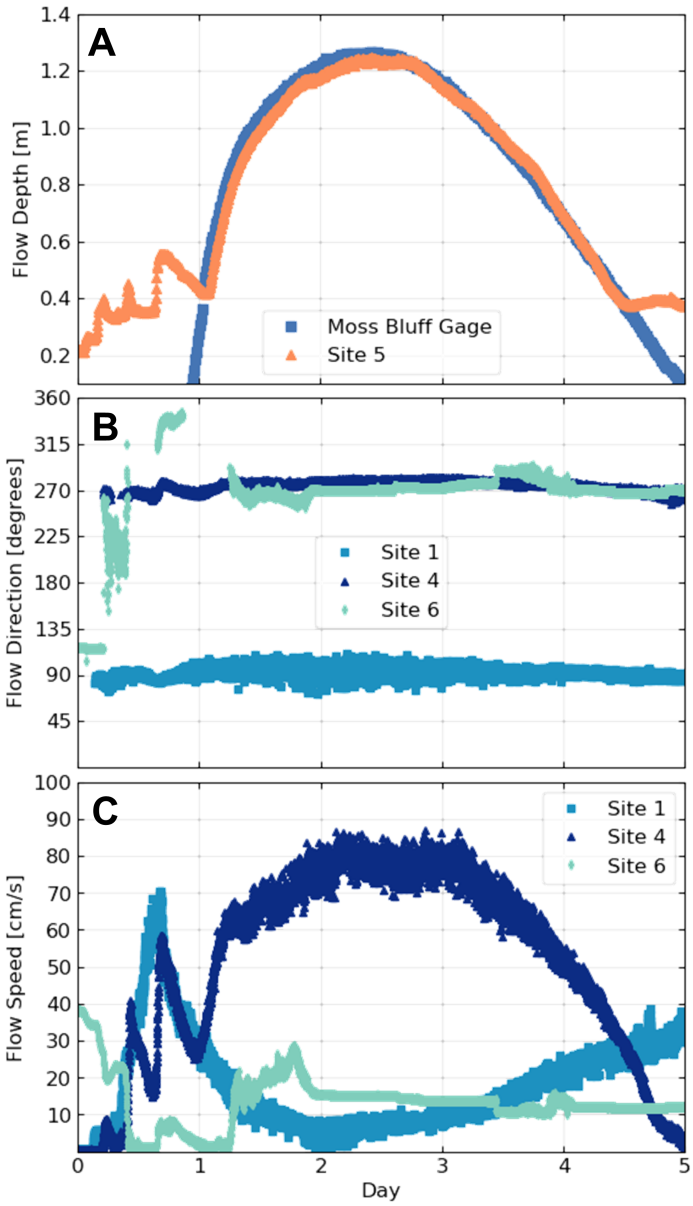

Figure 3. Flow patterns observed in field data in the Trinity River floodplain during Tropical Storm Imelda. (A) Water depths in the Site 5 floodplain channel, compared to river water levels at the nearby USGS gage (relative to the floodplain channel bottom). (B) Flow direction histories for three floodplain channels. Data are oriented so that 90 degrees aligns with flow out of channel and into river, and 270 degrees aligns with flow out of river and into floodplain. The channel at Site 1 always flowed out to the river, flow at Site 4 always flowed out onto the floodplain, and flow at Site 6 reversed direction during the rainfall phase. Flow directions are only plotted for velocities exceeding 5 cm/s. (C) Velocity histories at Sites 1, 4, and 6 were tied to competing water-level histories on the floodplain versus the river. At peak river stage, flow velocities toward the river at Site 1 are at a minimum, while flow velocities away from the river at Site 4 are maximum.

445 at this site due to proximity to the river and low elevation gradients; with an average annual
446 precipitation exceeding 1.3 m/yr, the water table on the floodplain remains high, within 1

m of the surface as confirmed by persistent standing water within local pools of floodplain channels. The saturated soil simplifies the analysis of pluvial flooding as any infiltration is small enough to be ignored without accruing measurable error. The complex flow patterns observed along the Trinity River during Imelda provided motivation to investigate the effect of rainfall on connectivity with numerical modeling and Lagrangian particle routing.

5.2 Numerical Modeling

The control model (20-m resolution) was calibrated to match the observed WSE at the USGS Moss Bluff gage. All models yielded similar results for WSE in the main channel at Moss Bluff (Figure 4A). The small differences in WSE at peak discharge are a product of the differences in lateral exchange that occur across models with different resolution. The high-resolution models have slightly lower WSE in the main channel than those with lower resolution, due to the increased exchange that occurs with more floodplain channels resolved.

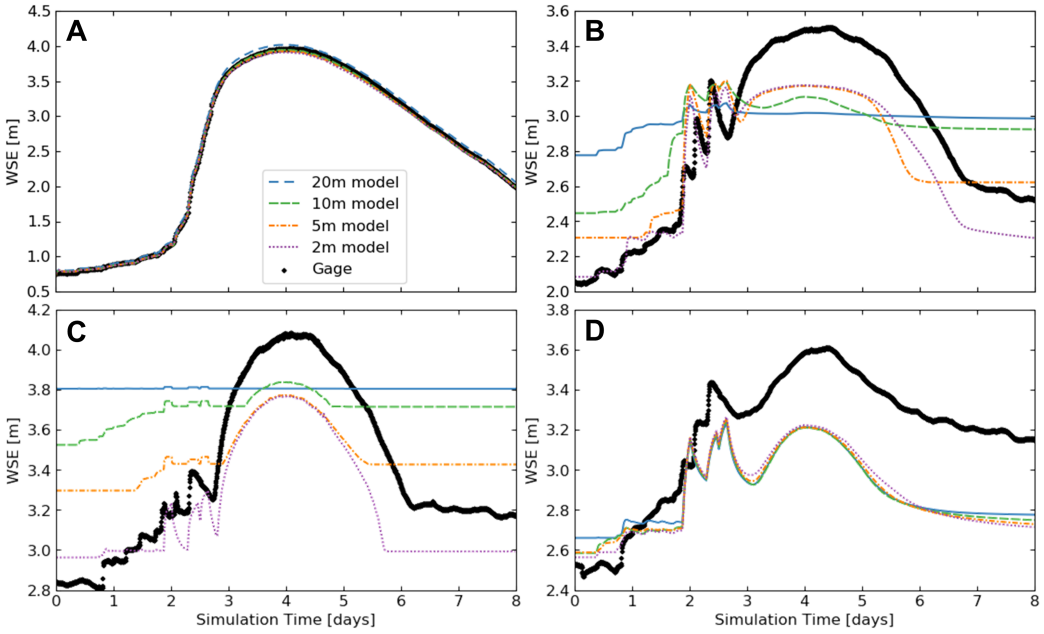

Figure 4. Numerical model results for models with local mesh resolution of 20 m, 10 m, 5 m, and 2 m. (A) WSE plot showing the match of each model to the stage measured at the USGS Moss Bluff gage. (B) Comparison of WSE measurements in the Site 4 floodplain channel to modeled WSE. (C) WSE comparison in the Site 5 floodplain channel. (D) WSE comparison at Site 6, at the terminus of the floodplain channel containing Site 5.

Depth measurements at Sites 4, 5 and 6 were converted to WSE by adding the depth to the lidar elevation at the GPS location of the instrument site. Model WSEs were then compared to measurements at the three sites (Figure 4B, C, and D). The flow patterns during the rainfall bands (hours 45-63) match the observations well, especially at Site 4 (Figure 4B), which is a wider and deeper channel than Site 5 (8-9 m compared to 4-5 m). However, all models show a mismatch in WSE during the river flooding phase. At Site 4, the shape of the WSE curve is modeled better with increasing resolution, but there appears to be an upper limit on depth in the floodplain channel. An elevation of 3.2 m is reached during the rainfall phase, followed by a brief drainage period, then another rising phase up to the same elevation of 3.2 m. The depth of this channel in the lidar is about 1 m, and the

WSE range for the 2-m model is also 1 m (Figure 4B), indicating that model flow depth is limited to the channel bankfull depth. Since the range of water levels recorded by the Site 4 instrument is close to 1.5 m, there is evidence that the actual depth of the channel is greater than indicated by the lidar.

Results are similar at Site 5 (Figure 4C). The shape of the fluvial signal is best matched by the 2-m model, but the measured depth in this floodplain channel is greater than in any of the models. Like Site 4, the effect of model resolution is most evident at the start of the simulation, where the 2-m model resolves the floodplain channel well compared to the lidar, and the 20-m model averages over the channel entirely. Unlike Site 4, where the 5-m model starting elevation is comparable to the 2-m model and lidar, the smaller channel width at Site 5 means the 5-m model does not resolve it as well. Site 5 results are also distinct in that higher resolution seems to reduce water levels by 5-10 cm in the floodplain channel. In the 10-m model, the channel is barely resolved, and there may be a bottleneck downstream in the floodplain channel from this lack of resolution. In the 2-m and 5-m models the channel may be resolved enough to convey flow more consistently.

There is essentially no difference among models at Site 6 (Figure 4D). The floodplain topography is mostly flat at this location, as it is located just beyond the terminus of a floodplain channel where it enters a small floodplain basin. But the nearly identical water levels may still describe the system of floodplain channels in some way, albeit indirectly. Rainfall accumulation in the floodplain is less dependent on the scales of connectivity along the river levees, but the fact that the same quantities of water reached this location in each model during the fluvial phase shows that, at this location and for this storm, river-floodplain connectivity is not dependent on channel size. In this case, the water is mostly supplied by the low-freeboard river bend located 500 m south-southwest of Site 6 (Figure 1C), which overtops across the entire bend beginning at about simulation hour 72.

Because the recorded water depths at the field sites were tied to the lidar rather than a datum, any error present in the lidar was passed to the measured data. This includes the 29-cm vertical accuracy of the lidar, which is similar to the WSE differences seen for Sites 4 and 5. It is possible that the differences are partially explained by lidar error, but considering that the model results are consistently lower by close to 30 cm, it is also possible that the sites had a combination of standing water and woody debris during the lidar flyovers. While the former is more likely, the presence of either element would alter the channel bottom elevations in the lidar and would artificially raise the measured depths plotted in Figure 4.

5.3 Particle Routing Analysis

Although the water depths in the floodplain did not exactly match the data, the flow patterns achieved in the numerical model followed many of the same trends, particularly for the high-resolution models. Using the numerical model flow fields for particle routing can help describe and quantify the complex interactions occurring in the floodplain during Tropical Storm Imelda. By continuously seeding passive particles in the river and floodplain, we can observe the differences between water moved by rainfall and river flooding, and how the dominant forcing changes in the floodplain during the storm. The analysis that follows is based on the ANUGA model with 5-m resolution unless otherwise noted, as the modeling results show that higher resolution improves the match of flow patterns to observations in the floodplain channels, but the improvement is not substantial between 5-m and 2-m resolution (Figure 4). More importantly, particle tracking results changed very little between flow grids derived from the 5-m and 2-m models.

5.3.1 Particle Dynamics in the Floodplain

Two particle classes were seeded continuously every 15 minutes throughout the storm event: one in the main channel and one distributed randomly throughout the floodplain. Floodplain particles were only seeded in grid cells where water had accumulated to a depth of 20 cm during the prior time step. Particle velocity distributions show the spatial extent of particle paths in two dimensions (Figure 5). During simulation hour 61 while it is still raining heavily, the gradient is from floodplain to river, and river particles remain confined, even though the floodplain is inundated everywhere except the topographic ridges (Figure 5A, seen in lighter shades of gray). At the same time, floodplain particle paths are widely connected (Figure 5D). At hour 72 (panels B and E) it is no longer raining heavily, but the peak river discharge has not arrived yet. Some of the rainwater has drained from the remote areas of the floodplain, and water pooled in the larger floodplain basins slows down (darker red colors) as it leaves through the outlet to the south. More river particles begin to enter the floodplain, mostly from the river bend due south of Site 6, but a few begin to enter through the floodplain channels near Site 4 as well. Finally, at hour 91 (panels C and F), the river discharge is at its maximum. Floodplain particles (panel F) are limited to the larger floodplain basins, similar to the previous time stamp, but average velocities are slightly higher overall. This is because the river is supplying more water to the floodplain, and thus providing a stronger gradient to the floodplain outlet that was not present at hour 72. As expected for particles originating in the river (panel C), the travel paths are limited to just a fraction of the floodplain, even during peak discharge. The combined average velocities across the entire duration (Figure 5G) show that river particle paths remain within the corridor shown in panels B and C throughout the simulation. The velocities show that river water generally spends less time in the floodplain than rainwater, with the exception of the floodplain in the north corner of the domain, which is highly-connected to the main channel and very deep (Figure 5G). The large, warm-colored region of lower floodplain particle velocities (Figure 5H) is inundated throughout the storm, but river particles never reach it. Instead, river particles seem to bypass this part of the floodplain entirely, while rainwater spends much more time in this area as it drains slowly to the outlet.

For river particles, residence time distributions (RTDs) were combined for cohorts seeded between hours 66 and 90, as there were not enough particles entering the floodplain at earlier times (Figure 6A). For floodplain particles, the combined time window is between hours 46 and 90 (Figure 6B). The limit at hour 90 was chosen because particles were only tracked up to hour 120, and the residence time window observed was limited to 30 hours. Ninety-five percent of river particles spent a minimum of five hours in the floodplain (within the model domain), and about 80 percent of particles had residence times less than 10 hours. The five percent of particles with residence times of less than five hours were those that entered the floodplain briefly before returning to the river. The narrower distribution confirms what can be seen spatially in the velocity distributions (Figure 5G). Floodplain particles had a wider distribution of residence times. Many particles exited the domain quickly if seeded close to the outlet, but 20 percent of floodplain particles remained in the domain for longer than 30 hours, compared to just 10 percent for river particles. Note that the river particle RTDs are composed of less particles by several orders of magnitude. Also note that the southeastern-most corner of the domain was masked out for the particle analysis because too many river particles were entering the floodplain at this bend and immediately exiting the floodplain due to proximity only, and this skewed the distributions.

Particle RTDs evolved over the course of the storm (Figure 6B and D). At hour 66, only a very small number of river particles entered the floodplain, but that number increased as the storm transitioned to the fluvial phase (Figure 6B). Through this transition, river particles experienced a reduction in minimum residence time and an increase in maximum residence time as the discharge increased. At higher discharges in the river, more flow moved through the floodplain, increasing velocities and reducing residence times. Conversely, activation of the floodplain channels near Site 4 at higher discharges brought particles into

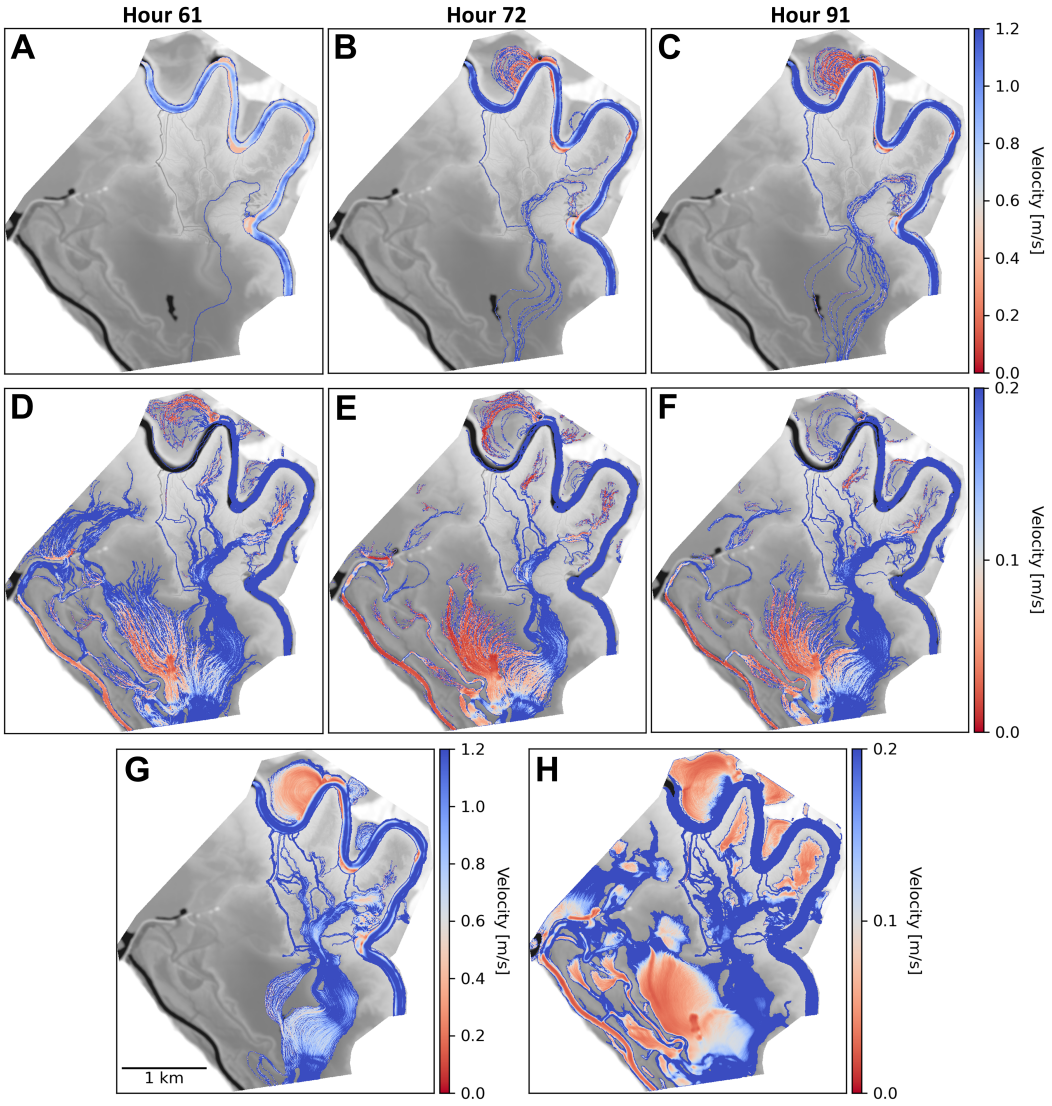

Figure 5. Average particle velocities for river particles (top row) and floodplain particles (second row). (A), (B), and (C) Velocity distributions for river particles at simulation hours 61, 72, and 91, respectively. (D), (E), and (F) Velocity distributions for floodplain particles at simulation hours 61, 72, and 91, respectively. Combined velocity distributions for (G) river and (H) floodplain particles.

the channels, creating longer flow paths than those that entered earlier from the bend near Site 6. The yellow and orange curves in Panel B imply that this was the case for about 20 percent of river particles.

Floodplain particle RTDs show a wider range of behavior, as there may be more competing factors involved in their movement (Figure 6D). The RTD for the earliest group of particle cohorts, representing most of the 8,000 particles seeded between hours 46 and 48, shows that 90 percent of particles left the floodplain after 15 hours. Fifteen hours corresponds to hour 61, when heavy rainfall was still active. Although the rainfall stops and starts twice during this 15-hour period, the overall period of rainfall flushed the floodplain to some degree, and the result is a nearly uniform distribution. Moving forward in time, the sixth group of cohorts (hours 56-58) marks a transition in the RTD where a greater

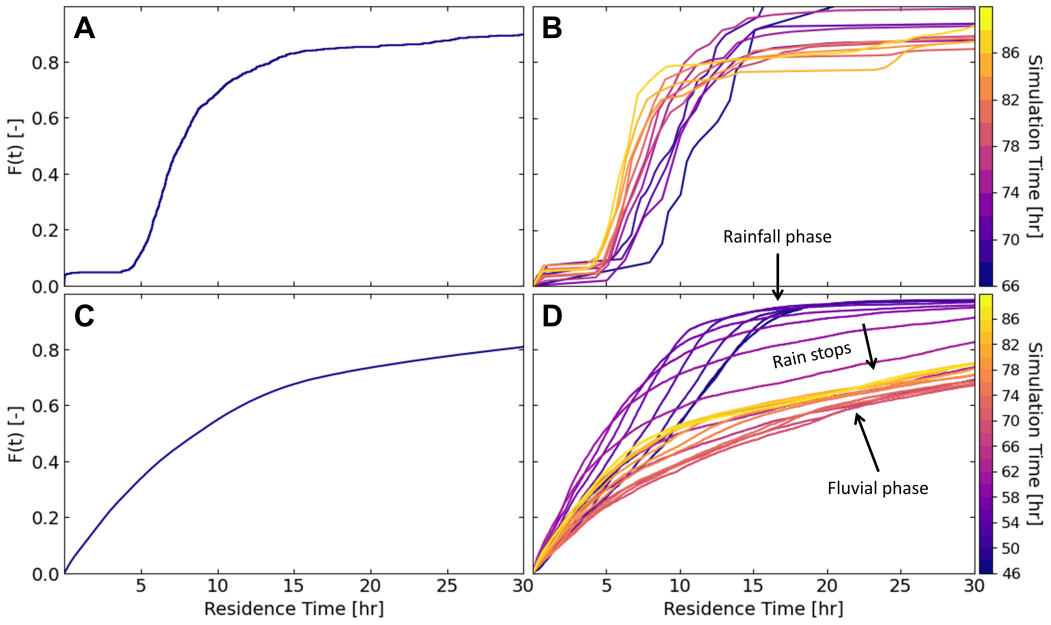

Figure 6. Cumulative Residence Time Distributions (RTDs) for river (top row) and floodplain (bottom row) particles. (A) Combined RTD for particles seeded in the river between simulation hours 66 and 90. (B) RTDs for river particles, grouped in intervals of two hours, where the darkest purple line is the combined RTD of particles seeded between hours 66 and 68, and the lightest yellow line represents particles seeded between hours 88 and 90. (C) Combined RTD for particles seeded in the floodplain between hours 46 and 90. (D) RTDs for floodplain particles. The darkest purple line represents particles seeded between hours 46 and 48, and the lightest yellow line represents particles seeded between hours 88 and 90.

fraction of particles left the floodplain faster, but the remaining particles spent longer than those from 10 to 12 hours prior. The transition can be attributed to the period between heavy rainfall and peak discharge. The longer residence times represent particles stranded in remote areas of the floodplain as rainwater drained, and the shorter residence times are a result of floodwaters accumulating closer to the outlet, where newly seeded particles then had less distance to travel to the outlet. Particle cohorts seeded between hours 56 and 62 began to show an increasingly greater fraction with shorter residence times, due to being seeded *after* the longest pause in rainfall (see Figure 2), but also an increasingly greater fraction with longer residence times, due to the heavy rainfall stopping for good after hour 63. After the rainfall phase, the RTD becomes more consistent through time, as the remote areas of the floodplain drain and inundation becomes dominated by river water. Average residence times reach a maximum (lowest red curves, Figure 6D) before reducing again during peak discharge when velocities are higher (bright yellow curves).

At field Site 6, located at the terminus of a floodplain channel in a small floodplain basin, a noteworthy reversal of flow occurred that was captured by the tilt current meter at the site (Figure 3B). A flow reversal at Site 6 was also observed in the model, albeit one with a slightly different pattern. The reversal can be well-described with particle routing. One hundred particles per 15 minutes were seeded at the Site 6 location. During the early rainfall phase, particles flowed directly to the floodplain outlet with a nearly constant residence time of five hours (Figure 7A and C, purple curves). After the rainfall stopped, flow paths remained similar, and residence times remained nearly constant at eight hours for 80-90 percent of particles. Beginning at about hour 76, as more river flow was conveyed to

the floodplain from the local floodplain channel and the bend to the south, the small basin began to fill up, causing new particles to become trapped there (Figure 7B and C, orange curves). This reversal lasted until about hour 88, very close in time to the peak discharge, when the floodplain basin water levels equilibrated with the river, and the flow direction reversed. Particles then returned to the original flow path, with nearly constant residence times of six hours for 90 percent of particles (Figure 7C, yellow curve). The flow reversal lasted for only 12 hours, but many particles seeded around this time had residence times exceeding 30 hours. In fact, the four groups of cohorts seeded between hours 78 and 86 had no particles with residence times less than 30 hours, while two particular RTD curves show the transition on either side of the flow reversal (Figure 7C, orange curves). Although only one local observation of flow reversal, it represents a drastic change in average residence times, and could have significant implications for floodplain processes when scaled to entire floodplain systems.

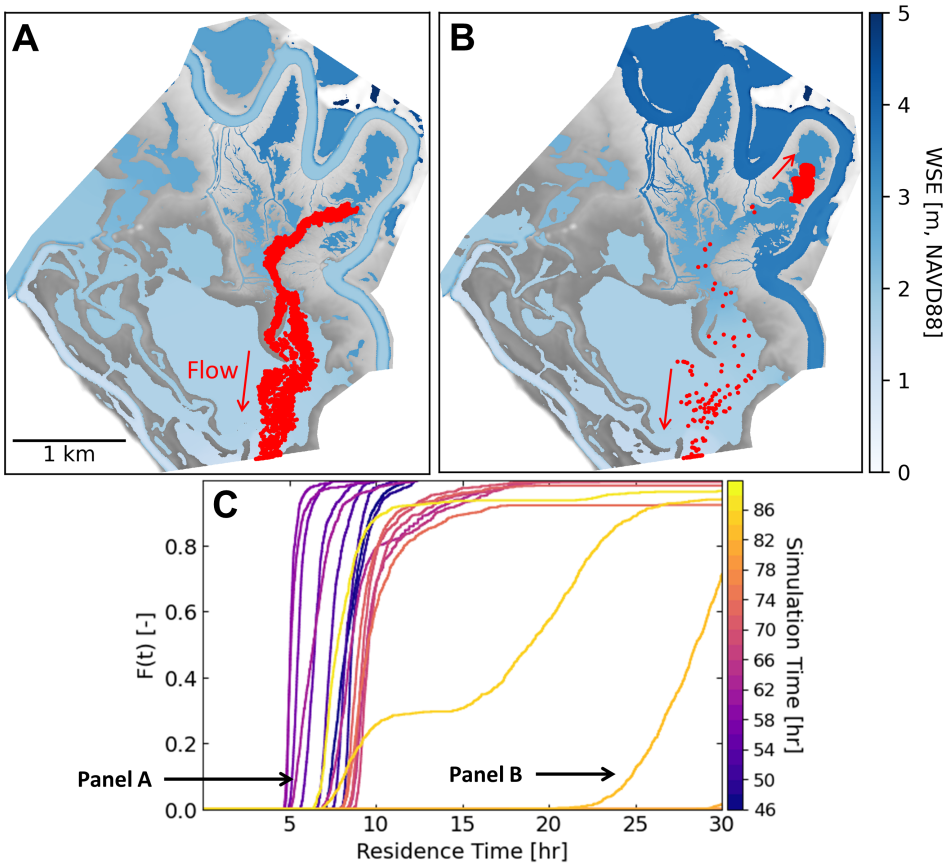

Figure 7. Flow patterns illustrated by particles seeded at Site 6. (A) State of particles at simulation hour 61. Heavy rainfall on the floodplain moved all particles toward the floodplain outlet. (B) State of particles at hour 89.5. Flow reversal due to fluvial flooding pushed particles farther into the scroll bar. The flow reversal lasted from hour 76 to hour 88, after which particles began flowing back toward the floodplain outlet. (C) RTDs for Site 6 particles grouped every two hours, from hour 46 (darkest purple curve) to hour 90 (lightest yellow curve). Six orange curves at the bottom right of the plot represent 12 hours of particles that experienced the flow reversal shown in panel B, four of which are completely flat.

5.3.2 Effect of Model Resolution

Hydrodynamics in the overall floodplain were largely unaffected by model resolution. The modeled WSEs at Site 6 (Figure 4D) showed that outside of floodplain channels there was little difference with higher resolution. There are locations in the model domain, such as the river bend near Site 6, where large amounts of water can move from river to floodplain on scales that are wider than the grid resolutions analyzed. The result is that floodplain residence times were very similar for model resolutions of 2 m, 5 m, and even 10 m (Figure 8A and B). For both particle classes, there was some difference observed with the coarser, 10-m resolution, but the general flow patterns were the same, and the major sources of river water to the floodplain were not dependent on changes in grid resolution below 10 m.

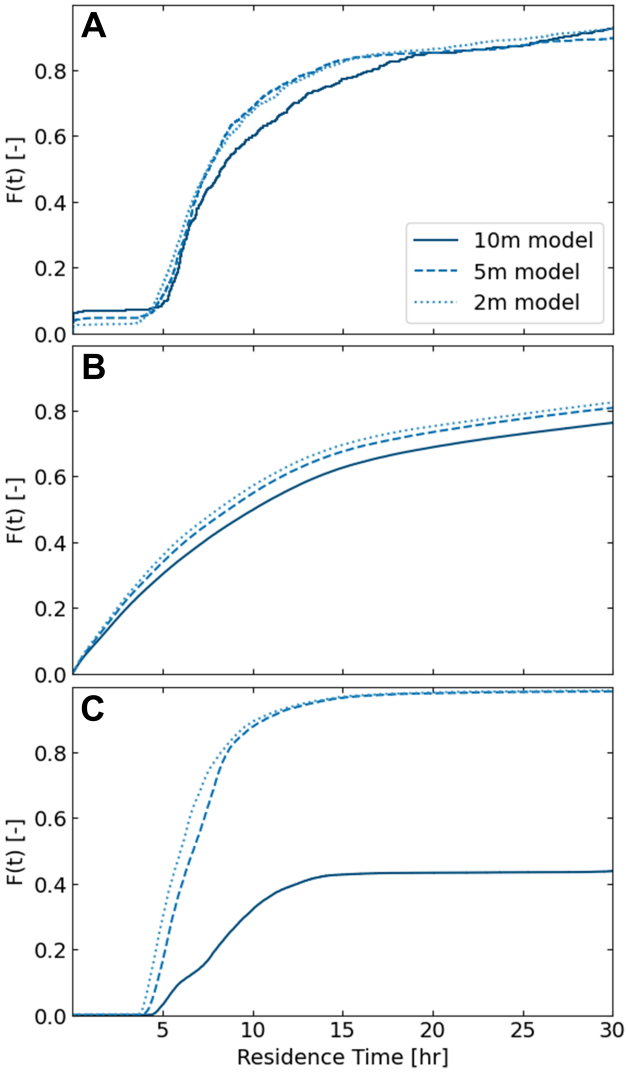

Figure 8. RTDs with different model grid resolutions, for (A) river particles released between hours 66 and 90, (B) floodplain particles released between hours 46 and 90, and (C) particles released in the Site 4 floodplain channel between hours 46 and 90. Flow processes in the overall floodplain were largely independent of grid resolution, but modeling local processes in floodplain channels requires a minimum resolution.

Particles released in the Site 4 floodplain channel showed that there can be a local resolution effect (Figure 8C). RTDs for the 2-m and 5-m resolution models were almost identical, but the 10-m model's failure to resolve the channel well completely changed the conveyance through the channel. Despite the fact that the majority of the floodplain beyond this local channel had a similar flow field in the model regardless of grid resolution, the under-resolved channel served as a local bottleneck for river flow. However, some fraction of particles still moved through the channel, even at 10-m resolution. Particle animations (see Supporting Information) showed that flow was only conveyed through this channel when rainfall was active, and directly following the peak discharge. During the pauses in rainfall, the flow drained from the channel and particles became stuck, to be flushed out when the rainfall resumed. Particles remained stuck in the channel for the period between heavy rainfall and peak discharge (hours 63-92), after which particles were conveyed through the floodplain due to sufficient river flow. Flow was cut off once again at hour 112. This result aligns with the range of WSE at this location in the 10-m model (Figure 4B), where the window of activity in the channel is much more limited. In general, the RTDs for Site 4 particles and the modeled WSE curves (Figure 4B and C) show the importance of model resolution on local processes where features near the scale of grid resolution are relevant.

The impact of model resolution can be seen in the channels close by to Site 4 as well. Field observations at Site 4 did not show any flow reversals as the event transitioned from rainfall to river-dominated (Figure 3B), and thus all particles released at Site 4 flowed south into the floodplain. But particle animations (see Supporting Information) showed that for particles released at Site 4 during the rainfall phase, a portion of flow was siphoned into the larger floodplain channel just west of Site 4, where local rainfall was moving water into the river. At the time when rainfall stopped, the flow reversed, and the gradual rise in river water levels did not allow particles to move into the river through these channels any longer. Particles only moved in this way with model resolution of 5 m or finer. The 10-m model could not resolve a deep enough floodplain channel to convey particles. Grid resolution is thus important for modeling flow through floodplain channels.

6 Discussion

6.1 Pluvial and Fluvial Flooding Interactions

Field data collected in the Trinity River floodplain during Tropical Storm Imelda provided strong evidence for flow bidirectionality between rivers and floodplains. The relative timing of rainfall and the peak discharge at the study site created an interesting transition of floodplain hydrodynamics from being pluvial-driven to fluvial-driven. The data showed that with heavy rainfall on the floodplain, river-floodplain connectivity can occur many hours (in this case about 24 hours) prior to the flood wave, and that this connectivity is influenced by floodplain channel topography. Furthermore, the extent of connectivity may be reduced or removed completely if rainfall intensity lessens or stops altogether for a period of time before peak river discharge. The data make clear that pluvial flooding can be an important component of river-floodplain connectivity.

For backwater systems such as the Trinity River, river discharges high enough to cause floodplain connectivity are more frequent than in upstream environments, although not as frequent as in deltas where lateral exchange can occur at all discharges (Hiatt & Passalacqua, 2017). Similarly, backwater floodplains are likely associated with high groundwater tables and saturated soil conditions, providing requisite conditions for pluvial flooding. The frequency of floodplain inundation, whether from rainfall or river discharge or both, indicates that a variety of floodplain processes are dependent on this connectivity, and unraveling some of the complexity can improve our understanding of the important hydrodynamic processes in floodplain ecosystems.

Numerical modeling and particle routing analysis reinforced many of the patterns seen in the data relating the timing mismatch of pluvial and fluvial flooding to bidirectional connectivity between the river and floodplain. Studies have shown that river-floodplain connectivity can be established at river stages less than bankfull (Mertes, 1997; Nicholas & Mitchell, 2003; Trigg et al., 2012; Czuba et al., 2019), but the current study showed that connectivity can be established from pluvial flooding at stages even less than the elevation of the deepest floodplain channels. In fact, model data and measurements from Site 1 show that heavy rainfall on a saturated floodplain can provide a competing force against river waters that would otherwise enter the floodplain. And while flow directed toward the river may only occur during a certain phase of a storm, even when a flow reversal occurs river flux into the floodplain may be limited by a reduced gradient from the presence of rainwater.

However, many areas of the floodplain can be activated by pluvial flooding that may not otherwise be reached by river water. If given enough time at peak discharge, river water may be able to reach more remote areas of the floodplain. But for events like Imelda where the discharge is sub-bankfull and the flood wave lasts for only a couple of days, river flooding is limited in time and space. Pluvial water may allow a hydraulic connection to form across a wider fraction of the floodplain, causing both a reduction in overall flow velocity in the basin from the deeper water and an opportunity for river water and its constituents to diffuse to more remote areas of the floodplain.

6.2 Implications for Nutrient Removal and Sediment Transport

Understanding the mechanisms controlling river-floodplain connectivity is important for understanding how many floodplain processes work. Floodplains, especially those near the coast, are known to act as sinks for nutrients present in river water, such as carbon and nitrogen (Tockner et al., 1999; Aufdenkampe et al., 2011; Noe et al., 2013; Wolf et al., 2013; Cheng & Basu, 2017), and for sediment (Tockner et al., 1999; Verhoeven et al., 2001; Schulz et al., 2003; Day et al., 2008; Juez et al., 2019). In some circumstances, floodplains can be a source of dissolved nutrients (Tockner et al., 1999). We have shown that pluvial flooding has a significant role in river-floodplain connectivity, and the implications for floodplain processes related to sediment retention and nutrient removal are numerous.

River-floodplain connectivity is typically studied as a process that is initiated from the river. In this framework, river water spreads into the floodplain over a range of sufficiently high discharges, bringing sediment and solutes to the floodplain. This study showed that there can be a competing gradient between fluvial and pluvial floodwaters, which may reduce the river water that moves into the floodplain, and thus reduce the transport of constituents to the floodplain where they are processed. When the river stage becomes high enough for flow to move into the floodplain, the presence of rainwater still impacts the dynamics. Velocity distributions (Figure 5) from particle routing analysis show that, for the domain studied, the reach of river water is limited to only a fraction of the floodplain. If there had been no rainwater in the floodplain, the river water and its constituents would have room to spread to a much larger area. Because the path of river particles is restricted to a relatively narrow corridor of the floodplain, residence times for river particles may be less than they otherwise would be. During peak discharge, RTDs showed that 80 percent of river particles move through the floodplain in about five to seven hours (Figure 6C). In contrast, particles randomly sampled in the floodplain during peak discharge show a much wider range of residence times depending on when and where they are seeded (Figure 6D). If we removed from consideration the fraction of sampled floodplain particles seeded close to the outlet, the distribution would be even wider. This result indicates that the active portion of the floodplain is within the corridor of river particle paths shown in the velocity distributions (Figure 5G), and the water in the remainder of the floodplain that mostly originated as rainwater is slower moving and less active (Figure 5H). So although inundation maps would show water throughout the floodplain, these results show that it is possible for river water

and its dissolved nutrients to short-circuit a large portion of the floodplain, potentially bypassing crucial floodplain ecosystem processes.

The routing parameters used in the particle analysis assume that each particle moves as a passive tracer. Particles, therefore, more closely represent solutes rather than sediment. However, sediment dynamics may be inferred from flow patterns, average velocities, and residence times in the floodplain. Similar to dissolved nutrients, sediment flux from river to floodplain is entirely dependent on the flow gradient, and it is less likely that floodplain sedimentation will occur if the dominant flow direction is toward the river. Again, floodplains already inundated with rainwater may reach equilibrium with the river more quickly, and reduce the window of time where sediment can be transported out of the river. For sediment that does enter the floodplain, sediment deposition is dependent on flow velocities and residence times, which in turn are dependent on the flow interactions that occur during the storm event. Residence times are shortest during peak rainfall and peak discharge when velocities are higher, but in between they can be significantly longer. So pluvial flooding can reduce overall river flow to the floodplain, but the increase in total floodplain volume due to rainwater may increase residence times. The dynamic nature of pluvial and fluvial compound flooding creates conditions for sediment transport and deposition that can change dramatically over the course of an event. In environments where pluvial flooding can be substantial, sediment dynamics should be considered and modeled within this context.

6.3 Floodplain Channel Scales and Model Resolution

In floodplain systems where connectivity is truly limited to smaller floodplain channels (during sub-bankfull flow conditions), grid resolution could be critical for modeling lateral exchange. The model domain used in this study was chosen partly because there were several floodplain channels of various scales present that had been shown by field observations to convey water in both directions. Model results showed that for processes in the overall floodplain, resolving those channels was not important. A large fraction of flow from the river was supplied by two river bends that were connected to the floodplain at low WSE and over length scales much larger than individual floodplain channels. Model results also showed that changes in flow magnitude and direction occur in these channels only when they are resolved sufficiently. Model resolution can then be important for understanding local processes, and could even be necessary for processes in the larger floodplain for systems where lateral exchange is completely limited to smaller topographic features.

For numerical modeling applications in other river-floodplain systems, or even other locations on the Trinity River, running low-cost model simulations prior to detailed investigation can provide guidance on the major sources of lateral exchange. In some systems it may be the case that the majority of floodplain connectivity is supplied from a small set of large breaches. While in most systems exchange is also likely to occur via smaller floodplain channels, it may not be on a large enough scale to affect overall flow patterns in the larger floodplain. For systems where it is known that floodplain channels are the main drivers of connectivity, it is necessary to resolve them with grid resolution finer than the scale of those channels. In either case, understanding which features are important in a system can allow modelers to shift computational resources to the most important aspects of their model.

6.4 Importance of Unsteady Modeling

This study described many ways in which floodplain flow patterns can change during a storm. Floodplains can experience periods of rapid pluvial accumulation, draining, flow reversal, and flow deceleration within the span of several days. The complexity of flow through the Trinity River floodplain during Tropical Storm Imelda shows that it is critical to model these processes in an unsteady way. For applications where the spatial extent of inundation is of interest for various discharges (e.g., Benke et al., 2000; Czuba et al., 2019), steady modeling of river-floodplain connectivity is appropriate. But for problems related

to sediment and solute transport into and out of the floodplain, it is crucial to understand how the spatial extent of inundation, flow time scales, and flow directions change over the course of a storm event.

6.5 Limitations and Future Work

The residence times computed in this study were useful for determining how travel times change with different hydrodynamic conditions. But the residence times are relative to the size of the model domain, and cannot be used to assess specific contact times needed for nutrient removal from the water column, for example. It is unclear what happens in the downstream floodplain, and how long water might stay there. It is likely that, for the same flow conditions, residence times change significantly moving down-valley through the lower Trinity River floodplains. It may be worthwhile to increase the model domain to a much larger river-floodplain reach. The domain used in this study needed to be small enough to meet computational constraints for the 2-m and 5-m simulations, but model results showed that large-scale floodplain processes may not depend on grid resolution at the scale of floodplain channels. A less costly numerical mesh that identifies critical topographic features beforehand may be sufficient to perform a similar study on a larger scale. At larger scales, we would expect to see floodplain flow rejoin the river at points downstream, and conclusions related to absolute residence times can be sought.

In addition to being limited in space, the particle analysis was also limited in time to just after the passing of the flood wave. The phase of the storm and associated floodplain dynamics related to the falling hydrograph limb and drainage from the floodplain was not analyzed here. We saw that particles in the floodplain slowed down after the period of intense rainfall ended (Figure 5D and E) and the floodplain began to drain. We also saw that residence times decreased during peak discharge as the total flow in the floodplain increased. It is expected that, following peak discharge, floodplain flow would slow down again as the forcing from the river decreases. This is an additional hydrodynamic phase not captured by the particle analysis, but one that could have implications for sediment deposition and nutrient retention.

The lidar data used for numerical modeling was collected in early 2017, and it is likely that the floodplain topography changed to some degree between then and field data collection (fall 2019). In fact, an even stronger storm (Hurricane Harvey) passed through the region after lidar was collected. Floodplain topography can change significantly over several years, which has been observed in Trinity River lidar data dating back to 2011 (Hassenruck-Gudipati, 2021). Combined with the possibility of lidar error in the floodplain channels, our numerical model results should be evaluated with these sources of error in mind. Still, the model was able to produce flow patterns that generally aligned with the patterns in the field data, and is therefore a useful tool for analyzing hydrodynamics in parts of the floodplain where no data was collected. Even if not an exact replicate of conditions during Tropical Storm Imelda, the relative timing and magnitude of pluvial and fluvial flooding applied to the model created unique conditions related to the competing flood modes that confirm at a larger spatial extent the observations made from the field data.

It is possible that the boundary condition imposed at the floodplain outlet is not representative of the conditions in the larger floodplain during Imelda. We imposed a dynamic, zero-momentum boundary with stage equal to the adjacent model floodplain stage during the previous time step. It is unclear whether this location saw more or less backwater during Imelda, and thus whether the rate of floodplain drainage in the model was accurate. Various boundary conditions were tested during the calibration phase (see Section 4.1), but this part of the floodplain was too low in elevation to have an impact on WSEs at any of the field sites for confirmation.

7 Conclusions

This study used field observations, numerical modeling, and Lagrangian particle routing to examine river-floodplain connectivity along the Trinity River during Tropical Storm Imelda. Field data and modeling showed the complex hydrodynamic interactions that can result from heavy pluvial flooding occurring in conjunction with high, sub-bankfull river flow. Floodplain residence times and flow directions in the floodplain can be strongly dependent on the dominant mode of flooding, and can change rapidly during a storm. Residence times were shorter during the periods of active rainfall and peak discharge, and flow slowed considerably in between these phases as flooding transitioned from pluvial to fluvial. Particle routing analysis showed that as river flow moved into a floodplain already inundated from rainwater, the spatial extent of river water was limited to a narrower reach of the floodplain. Without pluvial flooding, river water would likely spread farther into the floodplain where storage is available. Some floodplain channels were shown to facilitate two-way connectivity driven by the timing mismatch between pluvial and fluvial flooding. Although the 5 to 10-m floodplain channels in the study area were shown to be conveyors of lateral exchange, overall processes in the floodplain were unaffected by their resolution in the numerical model, as the majority of lateral exchange came from only a few locations. It is interesting to note that in this study, these bank-line locations are not bounded by levees, but rather are the sites of a previous cutoff of a river bend and the low-lying deposits of a counter point bar. Variability in how the bank line is constructed also plays an important role in river-floodplain connectivity.

The dynamic environment of competing pluvial and fluvial flooding during a storm has many implications for sediment and nutrient exchange between rivers and floodplains. The extent to which residence times and flow directions change indicates that optimal conditions for sediment deposition and nutrient retention are limited to only certain phases of a flood event. Enough pluvial flooding occurring prior to peak discharge may prevent river water from entering the floodplain altogether, effectively reducing sediment and nutrient fluxes to the floodplain. Pluvial flooding can also decrease velocities and increase residence times overall, as deep flow can be achieved sooner with less floodplain storage available for the peak river discharge. This study challenges the prevailing perspective that river-floodplain connectivity is dependent only on river discharge, and emphasizes the importance of rainfall as a driver of that connectivity.

Acknowledgments

This work was supported in part by fellowships from the Cockrell School of Engineering and the Graduate School at the University of Texas at Austin, and by the National Science Foundation (EAR-1350336). All modeling was performed using the Extreme Science and Engineering Discovery Environment (XSEDE), which is supported by National Science Foundation grant number ACI-1548562. Partial support for field data collection was provided by the Jackson School of Geosciences at the University of Texas at Austin. Lidar data were obtained from TNRIS, bathymetry data from the Trinity River Authority, and hydrological forcing data were obtained from USGS. The ANUGA (`https://github.com/GeoscienceAustralia/anuga_core`) and *dorado* (`https://github.com/passaH2O/dorado`) model codes are open-source and available online. If this manuscript is accepted, all codes and data currently provided in the Supporting Information will be made available in a public repository by the time of publication. The authors would like to acknowledge Andrew Moodie and Eric Prokocki for their feedback on this research. The authors report no conflicts of interest.

References

Alsdorf, D., Bates, P., Melack, J., Wilson, M., & Dunne, T. (2007). Spatial and temporal complexity of the Amazon flood measured from space. *Geophysical research letters*, *34*(8). doi: 10.1029/2007GL029447

Asselman, N. E. M., & Middelkoop, H. (1995). Floodplain sedimentation: Quantities, patterns and processes. *Earth Surface Processes and Landforms*, *20*(6), 481–499. doi: 10.1002/esp.3290200602

Aufdenkampe, A. K., Mayorga, E., Raymond, P. A., Melack, J. M., Doney, S. C., Alin, S. R., ... Yoo, K. (2011). Riverine coupling of biogeochemical cycles between land, oceans, and atmosphere. *Frontiers in Ecology and the Environment*, *9*(1), 53–60. doi: https://doi.org/10.1890/100014

Benjamin, M. M., & Lawler, D. F. (2013). *Water quality engineering: Physical/chemical treatment processes*. Hoboken, NJ: John Wiley & Sons, Inc.

Benke, A. C., Chaubey, I., Ward, G. M., & Dunn, E. L. (2000). Flood pulse dynamics of an unregulated river floodplain in the southeastern U.S. coastal plain. *Ecology*, *81*(10), 2730–2741.

Byrne, C. F., Stone, M. C., & Morrison, R. R. (2019). Scalable flux metrics at the channel-floodplain interface as indicators of lateral surface connectivity during flood events. *Water Resources Research*, *55*(11), 9788–9807.

Chen, X. C. L., Stone, M. C., & Acharya, K. (2020). Assessing connectivity between the river channel and floodplains during high flows using hydrodynamic modeling and particle tracking analysis. *Journal of Hydrology*, *583*, 124609. doi: 10.1016/j.jhydrol.2020.124609

Cheng, F. Y., & Basu, N. B. (2017). Biogeochemical hotspots: Role of small water bodies in landscape nutrient processing. *Water Resources Research*, *53*(6), 5038–5056. doi: 10.1002/2016WR020102

Chow, V. T. (1959). *Open-channel hydraulics*.

Covino, T. (2017). Hydrologic connectivity as a framework for understanding biogeochemical flux through watersheds and along fluvial networks. *Geomorphology*, *277*, 133–144. doi: 10.1016/j.geomorph.2016.09.030

Czuba, J. A., David, S., Edmonds, D. A., & Ward, A. S. (2019). Dynamics of surface-water connectivity in a low-gradient meandering river floodplain. *Water Resources Research*, *55*(3), 1849–1870. doi: 10.1029/2018WR023527

David, S. R., Edmonds, D. A., & Letsinger, S. L. (2017). Controls on the occurrence and prevalence of floodplain channels in meandering rivers. *Earth Surface Processes and Landforms*, *42*, 460–472. doi: 10.1002/esp.4002

Davies, G., & Roberts, S. (2015). Open source flood simulation with a 2D discontinuous-elevation hydrodynamic model. In *Proceedings of MODSIM 2015.*

Day, G., Dietrich, W. E., Rowland, J. C., & Marshall, A. (2008). The depositional web on the floodplain of the Fly River, Papua New Guinea. *Journal of Geophysical Research: Earth Surface*, *113*, F01S02. doi: 10.1029/2006JF000622

Gurnell, A. M., Corenblit, D., de Jalón, D. G., del Tánago, M. G., Grabowski, R. C., O'Hare, M. T., & Szewczyk, M. (2016). A conceptual model of vegetation–hydrogeomorphology interactions within river corridors. *River Research and Applications*, *32*(2), 142–163. doi: 10.1002/rra.2928

Hariharan, J., Wright, K., & Passalacqua, P. (2020). *dorado*: A Python package for simulating passive Lagrangian particle transport in shallow-water flows. *Journal of Open Source Software*, *5*(54), 2585. doi: 10.21105/joss.02585

Harvey, J., & Gooseff, M. (2015). River corridor science: Hydrologic exchange and ecological consequences from bedforms to basins. *Water Resources Research*, *51*, 6893-–6922. doi: 10.1002/2015WR017617

Hassenruck-Gudipati, H. J. (2021). *Understanding fluvial topography: Morphodynamic processes that build river levees and cut terraces* (Unpublished doctoral dissertation). The University of Texas at Austin, Austin, TX, USA. (115 pp.)

Hiatt, M., & Passalacqua, P. (2017). What controls the transition from confined to unconfined flow? Analysis of hydraulics in a coastal river delta. *Journal of Hydraulic Engineering*, *143*(6). doi: 10.1061/(ASCE)HY.1943-7900.0001309

Hughes, F. M. R., Adams, W. M., Muller, E., Nilsson, C., Richards, K. S., & et al., N. B. (2001). The importance of different scale processes for the restoration of floodplain

woodlands. *Regulated Rivers: Research & Management: An International Journal Devoted to River Research and Management*, *17*, 325–345. doi: 10.1002/rrr.656

Juez, C., Schärer, C., Jenny, H., Schleiss, A. J., & Franca, M. J. (2019). Rapid mapping of ultrafine fault zone topography with structure from motion. *Water Resources Research*, *55*(11), 9072–9091. doi: 10.1029/2019WR024989

Junk, W. J., Bayley, P. B., & Sparks, R. E. (1989). The flood pulse concept in river-floodplain systems. In G. P. Dodge (Ed.), *Proceedings of the International Large River Symposium. Canadian Special Publication in Fisheries and Aquatic Science* (Vol. 106, pp. 110–127).

Kondolf, G. M., Boulton, A. J., O'Daniel, S., Poole, G. C., Rachel, F. J., Stanley, E. H., ... Nakamura, K. (2006). Process-based ecological river restoration: Visualizing three-dimensional connectivity and dynamic vectors to recover lost linkages. *Ecology and Society*, *11*(2).

Kufel, L., & Leśniczuk, S. (2014). Hydrological connectivity as most probable key driver of chlorophyll and nutrients in oxbow lakes of the bug river (Poland). *Limnologica*, *46*, 94–98. doi: 10.1016/j.limno.2013.10.008

Kupfer, J. A., Meitzenand, K. M., & Gao, P. (2015). Flooding and surface connectivity of Taxodium-Nyssa stands in a southern floodplain forest ecosystem. *River Research and Applications*, *31*(10), 1299–1310. doi: 10.1002/rra.2828

Latto, A., & Berg, R. (2020). *Tropical Cyclone Report, Tropical Storm Imelda (AL112019) 17–19 September 2019* (Tech. Rep.). National Hurricane Center.

Lesack, L. F. W., & Melack, J. M. (1995). Flooding hydrology and mixture dynamics of lake water derived from multiple sources in an Amazon floodplain lake. *Water Resources Research*, *31*(2), 329–345. doi: 10.1029/94WR02271

Lewin, J., & Ashworth, P. A. (2014). The negative relief of large river floodplains. *Earth Science Reviews*, *129*, 1–23. doi: 10.1016/j.earscirev.2013.10.014

Liang, M., Geleynse, N., Edmonds, D. A., & Passalacqua, P. (2015). A reduced-complexity model for river delta formation - Part II: Assessment of the flow routing scheme. *Earth Surface Dynamics*, *3*, 87–104. doi: 10.5194/esurf-3-87-2015

Liang, M., Voller, V. R., & Paola, C. (2015). A reduced-complexity model for river delta formation - Part I: Modeling deltas with channel dynamics. *Earth Surface Dynamics*, *3*, 67–86. doi: 10.5194/esurf-3-67-2015

Mann, C. J., & Wetzel, R. G. (1995). Dissolved organic carbon and its utilization in a riverine wetland ecosystem. *Biogeochemistry*, *31*(2), 99–120.

Marriott, S. (1992). Textural analysis and modelling of a flood deposit: River Severn, UK. *Earth Surface Processes and Landforms*, *17*(7), 687–697. doi: 10.1002/esp.3290170705

Mason, J., & Mohrig, D. (2018). Using time-lapse lidar to quantify river bend evolution on the meandering coastal Trinity River, Texas, USA. *Journal of Geophysical Research: Earth Surface*, *123*(5), 1133–1144. doi: 10.1029/2017JF004492

Melack, J. M., & Forsberg, B. (2001). Biogeochemistry of Amazon floodplain lakes and associated wetlands. In M. E. McClain, R. L. Victoria, & J. E. Richey (Eds.), *Biogeochemistry of the Amazon Basin and its Role in a Changing World* (pp. 235–276). New York: Oxford Univ. Press.

Mertes, L. A. K. (1997). Documentation and significance of the perirheic zone on inundated floodplains. *Water Resources Research*, *33*(7), 1749–1762.

Mertes, L. A. K., Daniel, D. L., Melack, J. M., Nelson, B., Martinelli, L. A., & Forsberg, B. R. (1995). Spatial patterns of hydrology, geomorphology, and vegetation on the floodplain of the Amazon River in Brazil from a remote sensing perspective. *Geomorphology*, *13*(1-4), 215–232.

Mungkasi, S., & Roberts, S. G. (2011). A finite volume method for shallow water flows on triangular computational grids. In *Proc. 2011 Int. Conf. Advanced Computer Science and Information System (ICACSIS)* (pp. 79–84).

Mungkasi, S., & Roberts, S. G. (2013). Validation of ANUGA hydraulic model using exact solutions to shallow water wave problems. *Journal of Physics: Conference Series*,

423(1).

Nicholas, A. P., & Mitchell, C. A. (2003). Numerical simulation of overbank processes in topographically complex floodplain environments. *Hydrological Processes*, *17*, 727–746. doi: 10.1002/hyp.1162

Nielsen, O., Roberts, S., Gray, D., McPherson, A., & Hitchman, A. (2005). Hydrodynamic modelling of coastal inundation. In *Proceedings of MODSIM 2005.*

Noe, G. B., & Hupp, C. R. (2005). Carbon, nitrogen, and phosphorus accumulation in floodplains of Atlantic Coastal Plain rivers, USA. *Ecological Applications*, *15*(4), 1178–1190. doi: 10.1890/04-1677

Noe, G. B., Hupp, C. R., & Rybicki, N. B. (2013). Hydrogeomorphology influences soil nitrogen and phosphorus mineralization in floodplain wetlands. *Ecosystems*, *16*(1), 75–94. doi: 10.1007/s10021-012-9597-0

Park, E., & Latrubesse, E. M. (2017). The hydro-geomorphologic complexity of the lower Amazon River floodplain and hydrological connectivity assessed by remote sensing and field control. *Remote Sensing of Environment*, *198*, 321–332. doi: 10.1016/j.rse.2017.06.021

Pearson, K. (1905). The problem of the random walk. *Nature*, *72*(1867), 342–342.

Phillips, J. D., & Slattery, M. C. (2007). Downstream trends in discharge, slope, and stream power in a lower coastal plain river. *Journal of Hydrology*, *334*, 290–303. doi: 10.1016/j.jhydrol.2006.10.018

Phillips, J. D., Slattery, M. C., & Musselman, Z. A. (2004). Dam-to-delta sediment inputs and storage, lower Trinity River, Texas. *Geomorphology*, *62*(1–2), 17–34. doi: 10.1016/j.geomorph.2004.02.004

Roberts, S., Nielsen, O., Gray, D., Sexton, J., & Davies, G. (2015). ANUGA User Manual [Computer software manual].

Roley, S. S., Tank, J. L., & Williams, M. A. (2012). Hydrologic connectivity increases denitrification in the hyporheic zone and restored floodplains of an agricultural stream. *Journal of Geophysical Research: Biogeosciences*, *117*(G3).

Rowland, J. C., Dietrich, W. E., Day, G., & Parker, G. (2009). Formation and maintenance of single-thread tie channels entering floodplain lakes: Observations from three diverse river systems. *Journal of Geophysical Research: Earth Surface*, *114*(F02013). doi: 10.1029/2008JF001073

Schulz, M., Kozerski, H., Pluntke, T., & Rinke, K. (2003). The influence of macrophytes on sedimentation and nutrient retention in the lower River Spree (Germany). *Water Research*, *37*, 569–578. doi: 10.1016/S0043-1354(02)00276-2

Smith, V. B., Mason, J., & Mohrig, D. (2020). Reach-scale changes in channel geometry and dynamics due to the coastal backwater effect: the lower Trinity River, Texas. *Earth Surface Processes and Landforms*, *45*(3), 565–573. doi: 10.1002/esp.4754

Smith, V. B., & Mohrig, D. (2017). Geomorphic signature of a dammed sandy river: The lower Trinity River downstream of Livingston Dam in Texas, USA. *Geomorphology*, *297*, 122–136. doi: 10.1016/j.geomorph.2017.09.015

Tockner, K., Pennetzdorfer, D., Reiner, N., Schiemer, F., & Ward, J. V. (1999). Hydrological connectivity, and the exchange of organic matter and nutrients in a dynamic river–floodplain system (Danube, Austria). *Freshwater Biology*, *41*(3), 521–535. doi: 10.1046/j.1365-2427.1999.00399.x

Trigg, M. A., Bates, P. D., Wilson, M. D., Schumann, G., & Baugh, C. (2012). Floodplain channel morphology and networks of the middle Amazon River. *Water Resources Research*, *48*. (W10504) doi: 10.1029/2012WR011888

Verhoeven, J. T. A., Whigham, D. F., van Logtestijn, R., & O'Neill, J. (2001). A comparative study of nitrogen and phosphorus cycling in tidal and non-tidal riverine wetlands. *Wetlands*, *21*(2), 210–222. doi: 10.1672/0277-5212(2001)021[0210:ACSONA]2.0.CO;2

Ward, J. V., Tockner, K., & Schiemer, F. (1999). Biodiversity of floodplain river ecosystems: Ecotones and connectivity. *Regulated Rivers: Research and Management*, *15*, 125-139.

Wolf, K. L., Noe, G. B., & Ahn, C. (2013). Hydrologic connectivity to streams increases

nitrogen and phosphorus inputs and cycling in soils of created and natural floodplain wetlands. *Journal of Environmental Quality*, *42*(4), 1245–1255. doi: 10.2134/jeq2012.0466